Quantum chemical investigation of biexcitons in conjugated polymers

Melissa A. Pasquinelli and David Yaron*

Department of Chemistry, Carnegie Mellon University, Pittsburgh, PA 15213

Abstract

The formation of biexcitons in conjugated polymers is examined within the Pariser-Parr-Pople (PPP) model of polyacetylene. The calculations are done using a scattering formalism that provides a size-consistent description of excited states containing both single and double electron-hole pair excitations. The excited-state absorption spectrum from the 1^1B_u exciton state was calculated and examined for signatures of biexciton formation. Calculations were performed on polyenes with up to 9 unit cells, and on long chains using periodic boundary conditions. While polyenes with 7 to 31 unit cells exhibit states with some of the features expected for biexcitons, such states are not seen in the limit of long chains. This suggests that, within the two-band model considered here, exciton-exciton interactions are not of sufficient strength to lead to biexciton formation in the limit of long chains, and that their presence in shorter chains is due to confinement effects. In the long-chain limit, transitions are found to states consisting of overlapping electron-hole pairs, but these states have energies above that required to make two free excitons. These states may result from scattering resonances between excitons.

I. INTRODUCTION

The photophysical and semiconducting properties of conjugated polymers enable the construction of devices such as light-emitting diodes[1–4] and solid-state lasers.[5–9] But despite this functional similarity between organic and inorganic semiconductors, there are some significant differences in the details of the photophysics. Of particular interest here is the effective strength of Coulomb interactions between an electron and hole. Such interactions can lead to the formation of bound electron-hole pair states, or excitons. In conjugated polymers, estimates of the exciton binding energy range from 0.2 and 0.9 eV[10–16] which is much larger than the 10's of meV seen in inorganic semiconductors. So, unlike inorganic semiconductors, excitons play an important role in the room temperature photophysics of conjugated polymers. For instance, the 1^1B_u state of conjugated polymers is the lowest energy exciton state, and this state carries most of the one photon intensity out of the electronic ground state. Here, we examine the nature of the interaction between excitons and, in particular, whether such interactions can lead to binding between two excitons to form a biexciton state. These interactions may be especially important in applications that rely on high exciton densities such as solid-state lasers.[5–9]

Coherent many-particle states, such as biexciton states, are known to exist in inorganic semiconductors.[17] Although biexciton states have been observed in molecular aggregates[18] and charge transfer crystals,[19] their existence in other organic semiconductors remains uncertain. Several researchers have invoked biexcitons to account for features in the time resolved spectra of PPV oligomers[20–24]. However, a direct spectral transition to a biexciton state has yet to be observed. The photoinduced absorption spectrum of PPV does have a prominent feature at relatively high photon energy (1.4 eV), but assignment of this feature to biexcitons has been ruled out based on the unphysically large biexciton binding energy that would result from such an assignment[10,25,26]. Calculations performed on oligomers[10,25,27–39] suggest that biexcitons can exist in conjugated polymer chains. Since such calculations are difficult to perform on long polymer chains, results from oligomers are typically extrapolated to the long chain limit. While extrapolation typically yields an accurate depiction of the infinite chain for low lying excitations, this procedure can be problematic for high energy excitations.[40]

Because of chain length limitations and issues with size consistency,[32] our goal was to

develop a size-consistent technique that could be applied to long polymer chains in order to study high energy exciton-exciton interactions, including spectral signatures of biexcitons. This is accomplished by using the scattering formalism described in Section II. The Pariser-Parr-Pople (PPP) model of polyacetylene is used as a simple two-band model that captures the essentials of conjugated polymers. A Frenkel exciton model[41–44] is used as a benchmark for comparison, since the characterization of the biexciton within this model is fairly straightforward. Section III presents results obtained for oligomers, and for long chains with periodic boundary conditions. The excited-state absorption spectrum from the 1^1B_u exciton state is calculated and examined for signatures of biexciton formation. No such signatures are found in the long-chain limit of the PPP model. The results are summarized in Section IV.

II. FORMALISM

Much of the formalism used here was originally developed for nonresonant nonlinear optics, and a detailed justification of the approach and demonstration of its size consistency is given in Ref. 45. Here, we briefly describe the method and provide details on its application to the calculation of excited-state absorption spectra.

A. Hamiltonian

The calculations are performed on the Pariser-Parr-Pople (PPP)[46,47] model of polyacetylene. The molecular geometry is fixed, which prevents formation of solitons and makes this a simple two-band model that captures the salient features of conjugated polymers.

The PPP Hamiltonian models the π-electron system[48] by including one p orbital per carbon and assuming zero-differential overlap between these orbitals. The Hamiltonian can be written,

$$\begin{aligned}\hat{\mathrm{H}} \;=\; & \sum_i \left[-\mathrm{I} - \sum_{j\neq i} \Gamma_{i,j} \right] \hat{n}_i + \sum_{i,j,\sigma} \beta_{i,j}\, a^\dagger_{i,\sigma} a_{j,\sigma} \\ & + \tfrac{1}{2} \sum_i \Gamma_{i,i}\; (\hat{n}_i)\,(\hat{n}_i - 1) \\ & + \tfrac{1}{2} \sum_{i\neq j} \Gamma_{i,j}\; (\hat{n}_i - 1)\,(\hat{n}_j - 1), \end{aligned} \tag{1}$$

where $a^{\dagger}_{i,\sigma}$ and $a_{i,\sigma}$ are the creation and destruction operators for an electron with spin σ on the ith carbon atom, $\beta_{i,j}$ is the one-electron matrix element between electrons on carbons i and j, and $n_i = \sum_\sigma a^{\dagger}_{i,\sigma} a_{i,\sigma}$ is the number operator for electrons on carbon i. The calculations presented in this paper were performed on polyacetylene, with carbon-carbon double and single bond lengths of 1.35 and 1.46 $\mathring{A}$, and bond angles of 120°. One electron matrix elements are included between bonded carbon atoms, with β_1 =-2.5809 eV for double bonds and β_2 =-2.2278 eV for single bonds. The Coulomb energy is calculated using the Ohno parameterization,[49]

$$\Gamma_{i,j} \;=\; \frac{14.397 \text{ eV } \mathring{\text{A}}}{\sqrt{\left[\frac{14.397 \text{ eV } \mathring{\text{A}}}{U}\right]^2 + r_{i,j}^2}}, \tag{2}$$

where $r_{i,j}$ is the distance between the i^{th} and j^{th} orbitals and the Hubbard parameter U is 11.13 eV, the difference between the ionization potential and electron affinity in carbon.

The Hartree-Fock band structure and Wannier functions are obtained as described in Ref. 45. The Hartree-Fock solution yields one valence and one conduction band, and their corresponding Wannier functions.

B. Equation-of-Motion Method

The excited states contain electron-hole pairs created by promoting electrons from the valence to the conduction band. In Configuration Interaction (CI) theory, the excited states are written as linear combinations of various electron-hole configurations and the linear expansion coefficients are determined variationally. Size consistency is necessary for the energy to scale correctly with chain-length in the limit of a long chain. When only single electron-hole excitations are included (S-CI theory), the energy is size consistent. However, inclusion of double electron-hole pair excitations (SD-CI) leads to size inconsistencies that prevent proper convergence to a long-chain limit. To overcome this issue, we use an equation-of-motion (EOM) formalism, which has previously been shown to be size consistent.[45,50] This method differs from CI theory in that it constrains the ground state to remain the Hartree-Fock ground state. The excited electronic states can then be written,

$$\mid \text{excited state} \rangle \;=\; \Omega^{\dagger} \mid \text{HF} \rangle \,, \tag{3}$$

where $|\mathrm{HF}\rangle$ is the Hartree-Fock ground state, and $\Omega^\dagger$ is a linear combination of electron-hole pair creation operators. In the EOM method, the excitation operator $\Omega^\dagger$ describes only the difference between the ground and excited states, i.e. it is used only to create electron-hole pairs in the excited state.

In CI theory, the excitations are also used to describe electron-correlation in the ground electronic state, and it is this attempt to include ground-state correlation that leads to size inconsistencies. Due to Brillioun's theorem, whereby singles do not interact with the Hartree-Fock ground state, EOM and CI theory are equivalent at the singles level. The differences arise at the doubles level, and SD-EOM is useful since it provides a size-consistent description of excited states containing both single and double electron-hole pairs.

C. Periodic Boundary Conditions

We used periodic boundary conditions in order to study the limit of a long polymer chain. Due to the resulting translational symmetry, the excited electronic states may be written,

$$| \text{ excited state } \rangle \;\; = \;\; \frac{1}{\sqrt{N}} \sum_{n=1}^{N} e^{i\left(\frac{2\pi}{N}\right) K\, n} \; \Omega_n^{(K)\dagger} \;\; |\mathrm{HF}\rangle \,, \tag{4}$$

where the sum is over all N unit cells and K is the wave vector that describes the crystal momentum for the motion of the "center of mass" of the electrons and holes. $\Omega_n^{(K)\dagger}$ creates electrons and holes relative to the n^{th} unit cell, and describes the motion of the electrons and holes relative to one another. Due to the translational symmetry of the polymer, $\Omega_n^{(K)\dagger}$ has the same form on each unit cell, n, but its form is dependent on the crystal momentum K. The basis set for the excitation operator $\Omega_n^{(K)\dagger}$ is a factor of N smaller than the basis needed for an oligomer with the same number of unit cells. This reduction in basis set is the computational advantage of using translational symmetry.

To be consistent with periodic boundary conditions, the transition moment operator is that for a ring of polymer with N unit cells.[34,45] This leads to a selection rule $\Delta K = \pm 1$. The one-photon allowed states then have ${}^1B_u$ symmetry and $K = \pm 1$ while the two-photon allowed states have ${}^1A_g$ symmetry and $K = 0,\, \pm 2$.

D. Scattering Formalism

To obtain a size-consistent and computationally tractable description of the two-photon excited states, we employ the scattering formalism described in Ref. 45. This is an equation-of-motion approach (see Section II B), where the ground state is the Hartree-Fock ground state, the one-photon states are obtained from S-CI theory, and the two-photon states are obtained from SD-EOM theory.

The use of S-CI for the one-photon states and SD-EOM for the two-photon states gives a balanced description, such that states containing two excitons are treated with an accuracy that is equivalent to that used for the one-photon states. This balance is, for instance, necessary to obtain a size consistent description of two-photon optical processes.[45]

This need for a balanced description of the one and two photon states also influences the design of the contracted basis set in Section II F. Both the use of SD-EOM theory and the design of the contracted basis functions in Section II F assume that a biexciton can be well described by a local excitation consisting of up to double electron-hole pair excitations. The calculations presented here do not then test whether any excited state is present in the computed spectral regions. Rather, they test whether a state consisting of two interacting electron-hole pairs is present in these regions. In particular, covalent excitations such as the 2^1A_g state[48] may not be well-described by SD-EOM theory. The next highest level of theory in this scattering framework would use SD-EOM for the one-photon states, and a theory that includes up to quadruple excitations for the two-photon states. This would require development of a size-consistent approach to the inclusion of quadruple excitations. Also, the number of quadruple excitations scales as the seventh power of the number of unit cells, within periodic boundary conditions. This would likely limit the calculations to relatively small systems.

The excited-state absorption from the 1^1B_u state is calculated using,[51]

$$\chi^{(1)}(\omega) = \sum_a \frac{2\left|\mu_{ba}\right|^2 E_{ab}}{E_{ab}^2 - \left(\omega + i\Gamma\right)^2}, \tag{5}$$

where b is the 1^1B_u state obtained from S-CI theory, a is summed over all states obtained from the SD-EOM calculation, and Γ sets the linewidth. For the spectra shown in this report, Γ is set to a small value (0.01 eV) to allow all excited states to be resolved.

E. Frenkel Scattering Calculations

To aid interpretation of the spectra obtained from the PPP model (Section II A), we generate results for interacting Frenkel excitons using the model of Spano and coworkers.[41–44] An operator that creates a Frenkel exciton on the nth unit cell is defined as,

$$\hat{F}_n^\dagger = \frac{1}{\sqrt{2}} \left[a_n^\dagger \; b_n^\dagger + \bar{a}_n^\dagger \; \bar{b}_n^\dagger \right], \tag{6}$$

where $a_n^\dagger$ creates an electron and $b_n^\dagger$ creates a hole on the n^{th} unit cell and bars are used to indicate β as opposed to α spin. The Frenkel Hamiltonian can then be written,

$$\begin{aligned} \hat{\mathrm{H}} \; = \; & \sum_n \omega \, \hat{F}_n^\dagger \; \hat{F}_n - \sum_{n=1}^{N-1} J(\hat{F}_n^\dagger \; \hat{F}_{n+1} + c.c.) \\ & - \sum_{n,m} \frac{E_{\mathrm{exc-exc}}}{|n-m|^3} \, (\hat{F}_n^\dagger \; \hat{F}_m^\dagger \; \hat{F}_m \; \hat{F}_n), \end{aligned} \tag{7}$$

where ω sets the energy required to create a Frenkel exciton, J is the nearest neighbor hopping, $E_{\mathrm{exc-exc}}$ sets the strength of the dipole-dipole like interactions between excitons, and c.c. indicates complex conjugation. This model was parameterized to correspond to the PPP model by setting $\omega = 6.0$ eV and $J = 1.75$ eV. This value for J was chosen based on our previous calculations,[52] where the bandwidth of the exciton in the PPP model employed here was found to be 7 eV. Also note that biexciton formation should depend only on the dimensionless parameter $E_{\mathrm{exc-exc}}/J$, and this was confirmed in our implementation.

F. Contracted Scattering Calculations

In the scattering formalism of Section II D, S-CI theory is used for the one-photon states and SD-EOM theory is used for the two photon states. With periodic boundary conditions, the number of single electron-hole pair excitations scales as the number of unit cells, N, and so a complete set of all single excitations is included in both the S-CI and SD-EOM calculations. However, the number of double excitations grows as the third power of the number of unit cells.[55] To make the SD-EOM calculations tractable on long polymer chains, we use the contracted basis functions described in detail in Ref. 45 and summarized briefly here. This basis set implements a scattering approach for studying states containing two interacting excitons. We begin by defining an operator that creates a 1^1B_u exciton on the

n^{th} unit cell,

$$\hat{B}_n^{(K)\dagger} = \frac{1}{\sqrt{2}} \sum_{\delta=-m_{e-h}}^{m_{e-h}} c_\delta^{(K)} \left[a^\dagger_{n+x_c+\delta/2}\, b^\dagger_{n+x_c-\delta/2} + \bar{a}^\dagger_{n+x_c+\delta/2}\, \bar{b}^\dagger_{n+x_c-\delta/2} \right], \tag{8}$$

where $a_n^\dagger$ creates an electron on the n^{th} unit cell, and $b_n^\dagger$ creates a hole on the n^{th} unit cell. Bars are used to indicate β as opposed to α electron spin. The term in brackets creates a singlet-coupled electron-hole pair separated by δ unit cells and centered on the n^{th} unit cell if δ is even and centered between the n^{th} and $(n+1)^{th}$ unit cell if δ is odd (x_c is zero if δ is even and 1/2 if δ is odd). The coefficients, $c_\delta^{(K)}$ are determined through a S-CI calculation, with the (K) superscript indicating that the form of the 1^1B_u exciton depends on the crystal momentum K. Due to the binding between the electron and hole in an exciton, $c_\delta^{(K)}$ becomes small at large $|\delta|$. A local approximation can be implemented by setting $c_\delta^{(K)} = 0$ for $|\delta| > m_{e-h}$, as indicated by the limits on the summation in Eq. (8).

$\hat{B}_n^{(K)\dagger}$ then corresponds to the creation operator, $\Omega_n^{(K)\dagger}$ of Eq. (4), for a 1^1B_u exciton. The 1^1B_u state arises from the delocalization of this "effective particle"[45,52] as in Eq. (4),

$$\left|1^1B_u\right\rangle = \frac{1}{\sqrt{N}} \sum_{n=1}^{N} e^{i\left(\frac{2\pi}{N}\right)K\,n}\, B_n^{(K)\dagger}\ |\mathrm{HF}\rangle. \tag{9}$$

Here, it will be useful to include basis functions that describe the presence of two excitons on the polymer chain,

$$|\ \text{2-exciton}\ {}_\Delta\rangle = \frac{1}{\sqrt{N}} \sum_{n=1}^{N} \left[e^{i\left(\frac{2\pi}{N}\right)(K+K')n} \times \hat{B}_n^{(K)\dagger}\ \hat{B}_{n+\Delta}^{(K')\dagger} \right]\ |\mathrm{HF}\rangle\,, \tag{10}$$

which has the form of Eq. (4) with $\Omega_n^{(K)\dagger}$ creating two excitons, one centered on the n^{th} unit cell and one centered on the $(n+\Delta)^{th}$ unit cell. This basis function describes two excitons separated by Δ unit cells and delocalized with a crystal momentum that is the sum of that of the individual excitons, $K + K'$.

Eq. (10) is referred to as a contracted many-body basis function since it consists of a linear combination of a number of primitive electron-hole excitations. The coefficients of the linear combination are determined during construction of the basis set, via the S-CI calculation of $c_\delta^{(K)}$ in Eq. (8), and are not altered when using this basis set to obtain a variational solution of the Schroedinger equation. The use of contracted functions substantially reduces the

number of variational parameters, making it possible to affect a complete diagonalization of the Hamiltonian within the basis.

A scattering formalism is obtained by allowing interactions to alter the form of the excitons when the distance between the excitons is less than or equal to $n_{\rm scat}$ unit cells. Therefore, $n_{\rm scat}$ sets the size of the scattering region. To describe the excitons outside of the scattering region, the basis set includes the $\mid$ 2-exciton $_{\Delta}\rangle$ functions of Eq. (10), with $\Delta = n_{\rm scat} \ldots (N-1)$. Within the scattering region, we use a more complete basis of primitive electron-hole excitations. This is done by first constructing a primitive basis consisting of all single and double electron-hole pair excitations consistent with a maximum electron-hole pair separation of m_{e-h}. All primitives that are already present in the contracted functions ($|$2-exciton $_{\Delta}\rangle$; $\Delta = n_{\rm scat} \ldots N-1$) are then removed, and the remaining primitive functions provide a basis that describes the excitons within the scattering region.

The scattering calculations performed here do include interactions between excitons outside the scattering region. The approximation associated with the use of a scattering basis is that such interactions are not allowed to alter the form of the excitons outside the scattering region. When the scattering region is set to zero, $n_{\rm scat} = 0$, the form of the excitons is held fixed for all exciton-exciton separation distances. (No primitive double electron-hole pair functions are included in the basis and thus the interactions between excitons are not allowed to alter their form.) This case is then analogous to Frenkel exciton theory, except that the PPP Hamiltonian is used to explicitly calculate the interaction between the excitons. This exciton-exciton interaction is likely to be significantly more complicated than the form used for the Frenkel excitons in Section II E. For instance, the nature of the Pauli repulsion between excitons may be quite different. For Frenkel excitons, Pauli exclusion prevents the creation of two excitons on one unit cell. In the PPP model, the excitons are extended and, in creating the two-exciton contracted functions, the presence of the electron-hole pair in the first exciton restricts the possible locations of the electron-hole pair in the second exciton. The resulting Pauli exclusion interaction is most likely a repulsive interaction with a longer range than the hard-wall exclusion interactions between Frenkel excitons. As the size of the scattering region, $n_{\rm scat}$, is increased, exciton-exciton interactions are allowed to alter the form of the excitons. If the $n_{\rm scat} = 0$ calculations agree with the results obtained with a larger $n_{\rm scat}$, then a Frenkel-like model could be expected to capture the essentials of this system, although perhaps with a rather complex exciton-exciton interaction potential. To

the extent that the $n_{\rm scat} = 0$ calculation differs from the converged $n_{\rm scat}$ result, the scattering model has features which can not be described by Frenkel exciton theory.

III. RESULTS AND DISCUSSION

The primary goal of this research is to determine whether spectral signatures of biexcitons exist in the long chain limit. The spectra presented in this section are absorption from the 1^1B_u state to high-energy two-photon states, as described in Section II D. On a long chain, it should be possible to create two 1^1B_u excitons that are essentially non-interacting, and such states should have an energy twice that of the 1^1B_u state, $2 \times \mathrm{E}_{1^1\mathrm{B_u}}$. We therefore expect the absorption spectra calculated here to have an intense transition to a state near $2 \times \mathrm{E}_{1^1\mathrm{B_u}}$ in the limit of long chains. A spectral signature of a biexciton state is the appearance of a state at an energy below $2 \times \mathrm{E}_{1^1\mathrm{B_u}}$ whose wavefunction is characteristic of a bound state.

A. Frenkel Excitons

This section presents results from the Frenkel exciton model described in Section II E These results serve as a point of comparison for the PPP calculations presented below. Fig. 1 shows the excited state absorption spectra for a range of exciton-exciton interaction strength, $E_{\rm exc-exc}$, performed on a chain with 71 unit cells and periodic boundary conditions. The calculations indicate that for $E_{\rm exc-exc}$ greater than about 3 eV, or $E_{\rm exc-exc}/\mathrm{J} = 1.7$, a biexciton state breaks off from the two-exciton continuum. For all $E_{\rm exc-exc}$, transitions are observed to states at and above $2 \times \mathrm{E}_{1^1\mathrm{B_u}}$. For $E_{\rm exc-exc}$ greater than 3 eV, the formation of the biexciton is observed spectrally as a peak below $2 \times \mathrm{E}_{1^1\mathrm{B_u}}$.

Fig. 2 shows the analysis of the excited state wavefunctions for the states observed in the spectra for $E_{\rm exc-exc} = 2.0$ and 4.5 eV in Fig. 1. When $E_{\rm exc-exc} = 2.0$ eV, biexciton formation does not occur, as shown by the delocalized wavefunctions of Fig. 2. The number of nodes increases smoothly with energy, and the state energies follow the form expected for noninteracting particles-in-a-box (a least squares fit yields $E = 2.46\ eV + 0.021\ eV\ n^2$ for $n = 1 \ldots 5$). In the infinite chain limit, these states will form a continuum beginning at about 2.46 eV. This corresponds to the energy required to create an additional exciton on a long chain, and the value is essentially identical to the 2.5 eV required to create the first

exciton.

When $E_{\mathrm{exc-exc}} = 4.5$ eV, a biexciton state occurs at 2.09 eV. The wavefunction of this states indicates binding between the excitons with an average separation of about two to three unit cells. For the higher-energy states, the wavefunction is delocalized over the entire chain. The lowest unbound state (at 2.50 eV) has two nodes ($m_{\mathrm{exc-exc}} = 0$ and 3) and the number of nodes increases smoothly with increasing state energy. These higher energy levels fit a particle-in-a-box form ($E = 2.46\ eV + 0.026\ eV\ n^2$) with $n = 1$ being the 2.50 eV state. Just as for $E_{\mathrm{exc-exc}} = 2.0$ eV, these states will form a continuum beginning at 2.46 eV in the limit of an infinite chain. This indicates that the formation of a biexciton has little effect on the energy required to create two free excitons.

Similar results are obtained for Frenkel excitons on finite linear chains. Fig. 3 shows the 1^1B_u excited state absorption spectra for various chain lengths with exciton-exciton interaction above and below that required to support biexcitons on long chains. For $E_{\mathrm{exc-exc}}$ =2.0 eV, which does not support biexcitons on long chains, an intense transition occurs to a state containing two unbound excitons and this state approaches $2 \times \mathrm{E}_{1^1\mathrm{B_u}}$ from above. A number of states are also observed at higher energy, with intensity patterns that are not easily interpreted. For instance, these states do not fit the particle-in-a-box model used above for long chains with periodic boundary conditions. This complex behavior may arise from an interplay between the finite-chain boundary conditions and the exciton-exciton potential. For a value of $E_{\mathrm{exc-exc}}$ that leads to biexciton formation on long chains ($E_{\mathrm{exc-exc}}$=4.5 eV), the lowest energy transition shown in Fig. 3 arises from a biexciton state, as confirmed by analysis of the wavefunction. The energy of this biexciton state is relatively independent of chain length. Comparison of the $E_{\mathrm{exc-exc}} = 2.0$ and 4.5 eV spectra reveals that the biexciton state borrows intensity from the unbound two-exciton state. On short chains, $N = 9$ in Fig. 3, the biexciton carries essentially all of the intensity and the relative intensity to the two-exciton state increases rapidly with chain length. Just as for $E_{\mathrm{exc-exc}} = 2.0$ eV, the unbound two-exciton state approaches $2 \times \mathrm{E}_{1^1\mathrm{B_u}}$ from above, but the $E_{\mathrm{exc-exc}} = 4.5$ eV results show a much stronger dependence on chain length.

In comparing intensities, it is important to note that the intensities of the bound and free exciton states should scale differently with chain length in the long-chain limit.[39] The transition from a state with one exciton to a state with two unbound excitons corresponds to creation of an additional free exciton. Since there are $N-1$ locations for this second exciton

on a chain with N unit cells, the intensity should scale as N in the long chain limit. This is in contrast to the bound biexciton state, where the second exciton must be created next to the first exciton and so the number of possible locations is independent of chain length. (In effect, the biexciton acts a single effective particle and the transition corresponds to a conversion of the exciton into a biexciton, as opposed to the creation of an additional effective particle.) The transition from the 1^1B_u state to the biexciton state thus has an intensity that is independent of chain length in the long-chain limit. The spectra in Fig. 3 indicate that the intensity of the biexciton transition saturates by about 21 unit cells. The intensity of the free exciton transition increases rapidly with chain length, and begins to scale as N above about 41 unit cells.

The Frenkel exciton results of Fig. 1 allow us to examine the implications of using periodic boundary conditions within a well-understood model. This insight is useful since we must use periodic boundary conditions in order to investigate the long-chain limit of the PPP Hamiltonian. Fig. 1 shows a rather substantial difference between the K = 0 and K = 2 spectra, particularly in the region near $2 \times \mathrm{E}_{1^1\mathrm{B_u}}$. The splitting between the K = 0 and K = 2 transitions for the biexciton transition are as expected for a system in which the biexciton states form a band with a minimum at K = 0. However, in the vicinity of $2 \times \mathrm{E}_{1^1\mathrm{B_u}}$, the K = 0 and K = 2 spectra show differences that are not as easily rationalized. For instance, it is not clear why the lowest two peaks near $2 \times \mathrm{E}_{1^1\mathrm{B_u}}$ carry very different intensities for the K = 0 versus K = 2 spectra. Similar effects are observed in the PPP results of Section II F, and we take their presence within the Frenkel exciton model as evidence that this spectral feature is not indicative of complex exciton-exciton interactions. In particular, large difference between the K = 0 and K = 2 spectra are observed even for Frenkel excitons with no interactions ($E_{\mathrm{exc-exc}} = 0$) and with repulsive interactions ($E_{\mathrm{exc-exc}} =$ -4.5 eV). Also note that these are small splittings in a spectral region that will be dominated by one-photon absorption, and so are of no apparent experimental interest.

In summary, the results for Frenkel excitons indicate that excited-state absorption provides a good probe of biexciton formation. The biexciton appears as an intense transition below $2 \times \mathrm{E}_{1^1\mathrm{B_u}}$ and exhibits a weak dependence on chain-length.

B. PPP Oligomers

Fig. 4 shows excited-state absorption spectra for polyenes with between 4 and 9 unit cells. These were obtained from the PPP Hamiltonian using the scattering methodology of Section II D with a complete S-CI basis set for the one photon states and a complete SD-EOM basis set for the two photon states. Examination of Fig. 4 shows two classes of states.

The first class are the two states that have 48% and 64% double electron-hole pair character for N=9. The energy of these states decreases smoothly with increasing chain length, while the double electron-hole pair character remains relatively constant. In the Frenkel exciton calculations of Fig. 3, the states containing two unbound excitons approach $2 \times E_{1^1B_u}$ from above and have an intensity that increases with chain length. The lowest-energy state has an intensity that increases with chain length, suggesting two unbound excitons. However, two aspects of these states differ from the behavior expected for free exciton states. The first is that these states have significant contributions from single electron-hole pair configurations. The second is that the energy of the lowest of the two states drops below $2 \times E_{1^1B_u}$ for long chains, although the center of the two states does remain above $2 \times E_{1^1B_u}$. We attribute these states to mixtures between configurations involving two unbound excitons and configurations containing a single electron-hole pair.

The second class is the state with 89% double electron-hole pair character for N=9. The energy of this state also decreases smoothly with chain length, but with a dependence on chain length that is stronger than that of the first class, such that it crosses the lowest state of the first class between N=6 and N=7 and is not seen in the spectra for N<6. The large contribution from double electron-hole pair configurations, and the energy below that of the first class for N>7, suggests assignment to a biexciton. However, since the biexciton state is independent of chain length in the Frenkel model, the strong dependence on chain length observed here argues against a biexciton assignment. In any case, given the strong dependence of the energy of this state on chain length, examination of the long chain limit is desirable.

C. Long PPP Chains

In this section, we consider solutions of the PPP Hamiltonian on long chains of polyacetylene, using periodic boundary conditions and the scattering basis set of Section II F. This basis set restricts the maximum separation between the electron and hole in the exciton to 5 unit cells, $m_{e-h} = 5$ in Eq. (8). (Note that no such approximation was made in the finite chain calculations of Section III B.) This basis also defines a scattering region with size $n_{\rm scat}$ within which exciton-exciton interactions are allowed to alter the form of the excitons.

The convergence of the calculations with respect to the size of the scattering region, $n_{\rm scat}$, is depicted in Fig. 5. The behavior with increasing $n_{\rm scat}$ is fairly smooth, except for some discontinuous changes arising from mixing with single electron-pair configurations. For instance, the spectrum for $n_{\rm scat} = 2$ exhibits a transition near 2.3 eV that is not seen for any other value of $n_{\rm scat}$. This transition disappears when single electron-hole pair configurations are removed from the EOM calculation of the two-photon states (D-EOM), and is therefore attributed to mixing between a bright state that is predominantly double electron-hole pair in character and dark single electron-pair configurations. The peak at 2.3 eV arises only when $n_{\rm scat} = 2$ and is therefore an artifact of this particular value for the scattering region. This "mixing with background singles" occurs in a number of the calculated spectra presented in this section and is discussed in more detail below.

The spectra of Fig. 5 are well converged with respect to the size of scattering region, $n_{\rm scat}$. Although the higher energy transitions move about slightly in energy between $n_{\rm scat} = 5$ and 9, their intensities and relative positions are fairly well established. (The differences between $n_{\rm scat} = 8$ and 9 arise from mixing with background singles, as will be seen in the following detailed analysis of the $n_{\rm scat} = 9$ spectra.)

When $n_{\rm scat} = 0$, interactions between excitons are not allowed to alter their form. Since the results obtained for $n_{\rm scat} = 0$ do not agree with those for larger $n_{\rm scat}$, especially at high energy, we conclude that interactions between excitons alter their form in a manner that has consequences on the spectra. This suggests that a Frenkel exciton model, where interactions are not allowed to alter the form of the excitons, may not be sufficient to account for this high energy spectral region.

Fig. 6 shows the excited-state absorption spectra obtained with $n_{\rm scat} = 9$ on periodic chains with between 21 and 71 unit cells. Due to the use of periodic boundary conditions,

the calculated dependence on chain length may not reflect that of finite chains. This is especially true for small numbers of unit cells where large differences are observed between K = 0 and K = 2. The use of periodic boundary conditions should not effect the long chain limit of the spectrum, and so this is the focus of our analysis. The dependence on the number of unit cells is included primarily because it is a useful means to group transitions into classes and is therefore an aid to assignment of the long-chain limit.

Assignment of the long-chain limit of the spectrum is also aided by the results in Figs. 7 and 8 and Table I. Table I shows the contribution of single and double electron-hole pair configurations to the states giving rise to the transitions in the spectra of Fig. 6. Fig. 7 shows the probability density for the double electron-hole pair configurations as a function of exciton-exciton separation. (Since the separation between excitons can not be uniquely defined in the scattering region, the probability density is distributed uniformly throughout the scattering region in Fig. 7.) Fig. 8 shows the spectra obtained when only double electron-hole pair configurations are included in the calculation of the two-photon states (D-EOM). Comparison of Figs. 6 and 8 therefore shows the effects of single electron-hole pair excitations on the two-photon states.

This information allows us to group the excitations observed on long chains into three classes, which are discussed in turn below.

The first class of transitions are those that are most intense in the long chain limit, and are indicated by an (f), for free excitons, in Table I. These states consist primarily of double electron-hole pair configurations, having greater than 83% double electron-hole pair character for all chain lengths and greater than 97% double electron-hole character for chain lengths of 51 and above. Fig. 7 shows that the double electron-hole pair configurations consist of well separated excitons. These transitions are therefore assigned to states containing two unbound or free excitons. These states approach $2 \times \mathrm{E}_{1^1\mathrm{B_u}}$ in the limit of long chains, as expected for two free excitons. The K = 2 transition approaches $2 \times \mathrm{E}_{1^1\mathrm{B_u}}$ from above while the K = 0 transition approaches $2 \times \mathrm{E}_{1^1\mathrm{B_u}}$ from below. This behavior can be rationalized in terms of the selection rule for K (Section II C). Since the one-photon 1^1B_u state contains a single K = 1 exciton, $2 \times \mathrm{E}_{1^1\mathrm{B_u}}$ is the energy required for creation of two K = 1 excitons, or a two-exciton state with K = 2. We therefore expect the K = 2 unbound two-exciton state to approach $2 \times \mathrm{E}_{1^1\mathrm{B_u}}$ from above, due to the excluded volume interaction between the excitons. We also expect the K = 0 and K = 2 unbound two-exciton states to approach

one another in the limit of long chains. Both of these behaviors are, indeed, observed in the calculated spectra. The K = 0 transition approaches $2 \times E_{1^1B_u}$ from below because the splitting between the K = 0 and K = 2 states is larger than the shift due to the excluded-volume effect.

The most significant result in the long-chain limit of the spectrum is the absence of spectral features below the free exciton transition. This indicates that this system does not show spectral features due to biexciton states in the limit of long chains.

The second class of states are those labelled with an (x) in Figs. 6 - 8 and Table I. These states behave similarly to the higher-energy transitions of the Frenkel exciton model. Their energy decreases smoothly with increasing chain length, approaching that of the unbound exciton states discussed above. For K = 2, the states have greater than 90% double electron-hole pair character, and persist in the D-EOM spectra in Fig. 8, with slight shifts in energies and intensities. The analysis of the wavefunction in Fig. 7 for the 2.86 eV transition shows a nodal pattern similar to that seen for the second unbound exciton state in the Frenkel model of Fig. 2. The K = 0 spectra are similar, but exhibit two differences. One difference is that for $N = 51$, the K = 0 state appears to mix with background singles, giving rise to two transitions near 3.4 eV. This assignment to mixing with background singles is evidenced by both states having substantial contributions from single electron-hole pair configurations and there being only a single transition present in the D-EOM spectrum of Fig. 8. The other difference is that the wavefunction for the K = 0 state in Fig. 7 shows a more complex nodal pattern than that seen for K = 2, with two nodes being present outside of the scattering region. Nevertheless, it seems reasonable to assign both the K = 0 and K = 2 transitions of this class to states containing unbound excitons. By analogy with similar states in the Frenkel exciton model, we expect these higher-energy unbound exciton states to converge onto the lowest-energy unbound exciton states in the limit of an infinite chain.

The third class of states are the K = 0 states labelled with a (*) and the K = 2 states labelled with a (+) in Figs. 6 - 8 and Table I. These states are grouped together based on their similar and smooth change in energy with increasing chain length, and their similar wavefunction decompositions in Table I. Fig. 7 reveals that the probability density arising from the double electron-hole pair configurations lies predominantly in the scattering region. We therefore assign these transitions to either overlapping excitons or to some other type of two-photon allowed state in which two electrons and two holes are bound together into

a single effective particle. If these states do arise from overlapping excitons, their location above the energy of two free excitons is indicative of a scattering resonance rather than a biexciton.

The overlapping exciton states mix with background singles to give two transitions for K = 0, labelled with a (*), and two transitions for K = 2, labelled with a (+), in Fig. 6. This assignment to mixing with background singles is supported by Table I, which shows that these states have significant contributions from single electron-hole pair configurations. Also, in the D-EOM spectra of Fig. 8, only a single transition of this type is observed for each value of K. This suggests that the overlapping exciton state mixes with single electron-hole pair configurations, leading to the two transitions in the SD-EOM spectra in Fig. 6. Fig. 5 indicates that this mixing with background singles occurs for $n_{\rm scat} = 9$ but not for $n_{\rm scat} = 6$ - 8.

Mixing with background singles was invoked three times in the above analysis. In each case, the mixing only appeared for specific values of the model parameters ($n_{\rm scat} = 2$ for the 2.3 eV transition of Fig. 5, a chain length of 51 unit cells for the K = 0 higher-energy free exciton transition of class (x), and $n_{\rm scat} = 9$ for the overlapping exciton peaks of class (*) and (+)). This suggests that the mixing arises when a single electron-hole pair configuration happens to be in close resonance with the double electron-hole pair state that carries the two-photon intensity. It seems unlikely that the mixing with background singles, observed in these calculations, will be reflected in the real system. For the model used here, the density of single electron-hole pair excitations is fairly low; a S-CI calculation on a periodic system with 71 unit cells gives about 4 states in the energy range of Fig. 6 for each value of crystal momentum, K. Since this energy range is above the exciton binding energy, the single electron-hole pair states will become a continuum in the long-chain limit[56] and this will likely remove the resonances. Even if such resonances still remain in the long-chain limit, the amorphous nature of conjugated polymers films seems likely to average away their effects on the spectra.

We therefore view the mixing with background singles as an aspect of the calculations that is not of relevance to the actual system. The above results can therefore be summarized as showing states containing free excitons, that behave similarly to that of unbound Frenkel excitons, and states containing two overlapping electron-hole pairs, whose energy is above that of the lowest free exciton state.

Due to the use of periodic boundary conditions, the spectra of Fig. 6 are only reliably connected to that of a finite chain in the limit of long chains. Nevertheless, the chain length dependence of Fig. 6 may give some insight into the effects of confining two excitons to a small region. As the chain length decreases, the energy of the overlapping excitons (the states labelled (*) and (+) in Figs. 6 and 8) decreases, while the energy of the $2 \times E_{1^1B_u}$ transition increases. Eventually the overlapping exciton state crosses the $2 \times E_{1^1B_u}$ state such that the overlapping excitons lie lower in energy than the free excitons. This suggests that spatially confining excitons can lead to biexciton formation. This may account for the double electron-hole pair state observed in the finite chain calculations of Fig. 4. For a finite chain with 9 unit cells, the double electron-hole pair state appears about 0.5 eV below $2 \times E_{1^1B_u}$. A similar biexciton binding energy is observed in the periodic system with 21 unit cells, where the overlapping exciton transitions occur about 0.5 eV below $2 \times E_{1^1B_u}$.

IV. SUMMARY

This calculations presented here explore the existence of biexciton states in conjugated polymers, using the PPP Hamiltonian of polyacetylene as a simple two-band model of these materials. The excited state absorption spectrum from the 1^1B_u state is calculated as a probe of the biexciton states. This approach to identifying biexcitons was verified using a Frenkel exciton model as a benchmark system. In the Frenkel model, a biexciton state is formed above some critical exciton-exciton interaction strength. This biexciton state has an energy below that of $2 \times E_{1^1B_u}$ and carries significant intensity from the 1^1B_u state, such that it is readily identified in the excited state absorption spectrum.

On finite chains with between 7 and 9 unit cells, states are observed below $2 \times E_{1^1B_u}$ that are dominated by double electron-hole pair configurations. While this is suggestive of a biexciton state, the energy of this double electron-hole pair state decreases rapidly with chain length. This is in contrast to the Frenkel exciton model, where the biexcitons are relatively independent of chain length. To explore the existence of a biexciton state in the long-chain limit, calculations were done on large systems using periodic boundary conditions and the scattering methodology discussed in Sec. II F. When the size of the scattering region is set to zero, the scattering formalism is analogous to a Frenkel exciton model in that exciton-exciton interactions are not allowed to alter the form of the excitons. However, it differs from the

Frenkel model in that it uses the PPP Hamiltonian to explicitly calculate the exciton-exciton interactions. It also includes the finite size of the excitons and the resulting Pauli-exclusion interactions between excitons. As the size of the scattering region is increased, exciton-exciton interactions are allowed to alter the form of the excitons when the exciton-exciton separation is less than the size of the scattering region. Convergence is observed for a scattering region of about 6 unit cells. The need for a large scattering region suggests that a Frenkel exciton model is not sufficient to describe the states that arise in the high-energy region above $2 \times E_{1^1B_u}$.

The principal result of the scattering calculations is the absence of spectral signatures of biexcitons in the long-chain limit. States are seen above $2 \times E_{1^1B_u}$ that have a large contribution from two overlapping electron-hole pairs. If these states are attributed to overlapping excitons, their existence above $2 \times E_{1^1B_u}$ is suggestive of a scattering resonance rather than a bound biexciton state. Within periodic boundary conditions, decreasing the length of the chain causes the energy of this overlapping electron-hole pair state to drop below $2 \times E_{1^1B_u}$. Finite chains with between 7 and 9 unit cells also exhibit states below $2 \times E_{1^1B_u}$ that are dominated by double electron-hole pair configurations. These results suggest that confinement of excitons can lead to biexciton formation.

The results presented here reflect the nature of exciton-exciton interactions within a restricted but reasonable model of conjugated polymers. The model assumes a single valence and conduction band, with electron-hole interactions calculated via the PPP Hamiltonian. Since the geometry is frozen, which suppresses soliton formation, and dielectric screening of electron-hole interactions is not included, this model corresponds to a fairly large exciton binding energy (>2.5eV)[53,54]. The scattering formalism further assumes that excitons consist of single electron-hole pair configurations and biexcitons consist of a mixture of single and double electron-hole pair configurations. The model therefore explores the states resulting from placing one or two electron-hole pairs on a periodic chain. The results indicate that biexciton formation does not occur on long chains, although it may be present in confined systems. If biexciton formation does occur in long-chain conjugated polymers, it must arise from effects not included in this model, such as the presence of multiple bands, deviation of the electron-hole interaction potential from that of the PPP Hamiltonian, or the contribution of more highly excited electron-hole pair configurations to the exciton or biexciton states.

V. ACKNOWLEDGMENTS

This work was funded by the National Science Foundation CHE9985719.

* Electronic address: yaron@chem.cmu.edu

[1] M. Strukelj, F. Papadimitrakopoulos, T. M. Miller, and L. J. Rothberg, Science (Washington, D. C.) **267**, 1969 (1995).

[2] R. H. Friend et al., Nature (London) **397**, 121 (1999).

[3] G. Kranzelbinder et al., Appl. Phys. Lett. **71**, 2725 (1997).

[4] U. Mitschke and P. Bauerle, Journal of Materials Chemistry **10**, 1471 (2000).

[5] N. Tessler, G. J. Denton, and R. H. Friend, Nature **382**, 695 (1996).

[6] F. Hide et al., Science **273**, 1833 (1996).

[7] F. Hide, M. A. Diaz-Garcia, B. J. Schwartz, and A. J. Heeger, Acc. Chem. Res. **30**, 430 (1997).

[8] T. Kondo, T. Azuma, T. Yuasa, and R. Ito, Solid State Commun. **105**, 253 (1997).

[9] N. Tessler, Adv. Mater. (Weinheim, Ger.) **11**, 363 (1999).

[10] J. M. Leng et al., Phys. Rev. Lett. **72**, 156 (1994).

[11] I. H. Campbell, T. W. Hagler, D. L. Smith, and J. P. Ferraris, Phys. Rev. Lett. **76**, 1900 (1996).

[12] R. N. Marks et al., J. Phys., Condens. Matter **6**, 1379 (1994).

[13] M. Deussen, M. Scheidler, and H. Bassler, Synth. Met. **73**, 123 (1995).

[14] M. Chandross et al., Phys. Rev. B **50**, 14702 (1994).

[15] P. G. da Costa and E. M. Conwell, Phys. Rev. B **48**, 1993 (1993).

[16] Z. Shuai, J. L. Bredas, and W. P. Su, Chem. Phys. Lett. **228**, 301 (1994).

[17] H. Haken and S. Nikitine, Excitons at High Density, Springer Tracs Mod. Phys. (Springer-Verlag, New York, 1975).

[18] A. Chakrabarti et al., Phys. Rev. B **57**, 4206 (1998).

[19] M. Kuwata-Gonokami et al., Nature (London) **367**, 47 (1994).

[20] V. I. Klimov, D. W. McBranch, N. Barashkov, and J. Ferraris, Phys. Rev. B **58**, 7654 (1998).

[21] V. Klimov, D. McBranch, N. Barashkov, and J. Ferraris, Proc. SPIE-Int. Soc. Opt. Eng. **3145**, 58 (1997).

[22] V. I. Klimov, D. W. McBranch, N. N. Barashkov, and J. P. Ferraris, Chem. Phys. Lett. **277**, 109 (1997).

[23] B. Kraabel and D. W. McBranch, Chem. Phys. Lett. **330**, 403 (2000).

[24] B. Kraabel et al., Phys. Rev. B: Condens. Matter Mater. Phys. **61**, 8501 (2000).

[25] J. M. Leng et al., Mol. Cryst. Liq. Cryst. Sci. Technol., Sect. A **256**, 1 (1994).

[26] A. Chakrabarti and S. Mazumdar, Phys. Rev. B **59**, 4839 (1999).

[27] F. Guo, M. Chandross, and S. Mazumdar, Phys. Rev. Lett. **74**, 2086 (1995).

[28] M. Chandross, F. Guo, and S. Mazumdar, Synth. Met. **69**, 625 (1995).

[29] F. Guo, M. Chandross, and S. Mazumdar, Mol. Cryst. Liq. Cryst. Sci. Technol., Sect. A **256**, 53 (1994).

[30] S. Mazumdar et al., J. Chem. Phys. **104**, 9292 (1996).

[31] M. Chandross, Y. Shimoi, and S. Mazumdar, Chem. Phys. Lett. **280**, 85 (1997).

[32] V. A. Shakin and S. Abe, Phys. Rev. B **50**, 4306 (1994).

[33] S. Abe, Y. Shimoi, V. A. Shaken, and K. Harigaya, Mol. Cryst. Liq. Cryst. Sci. Technol., Sect. A **256**, 97 (1994).

[34] F. B. Gallagher and F. C. Spano, Phys. Rev. B **53**, 3790 (1996).

[35] F. C. Spano, Chem. Phys. Lett. **234**, 29 (1995).

[36] F. B. Gallagher and F. C. Spano, Synth. Met. **85**, 1007 (1997).

[37] K. Ishida, H. Aoki, and T. Ogawa, Phys. Rev. B: Condens. Matter **52**, 8980 (1995).

[38] Z. G. Yu et al., Phys. Rev. B: Condens. Matter **52**, 4849 (1995).

[39] S. Pleutin, Phys. Rev. B: Condens. Matter Mater. Phys. **61**, 4554 (2000).

[40] S. Mazumdar, D. Guo, and S. N. Dixit, J. Chem. Phys. **96**, 6862 (1992).

[41] F. C. Spano and J. Knoester, Adv. Magn. Opt. Reson. **18**, 117 (1994).

[42] F. C. Spano, Phys. Rev. Lett. **67**, 3424 (1991).

[43] F. C. Spano, Physical Review B **46**, 13017 (92).

[44] F. C. Spano and E. S. Manas, J. Chem. Phys. **103**, 5939 (1995).

[45] D. Yaron, Phys. Rev. B **54**, 4609 (1996).

[46] R. Pariser and R. G. Parr, J. Chem. Phys. **21**, 466 (1953).

[47] J. A. Pople, Trans. Faraday Soc. **49**, 1375 (1953).

[48] I. Ohmine, M. Karplus, and K. Schulten, J. Chem. Phys. **68**, 2298 (1978).

[49] K. Ohno, Theor. Chim. Acta **2**, 219 (1964).

[50] D. Yaron, Mol. Cryst. Liq. Cryst. **256**, 631 (1994).

[51] S. Mukamel, Principles of Nonlinear Optical Spectroscopy (Oxford University Press, New York, 1995).

[52] M. A. Pasquinelli and D. Yaron, Synth. Met. **101**, 518 (1999).

[53] E. Moore, B. Gherman, and D. Yaron, J. Chem. Phys. **106**, 4216 (1997).

[54] E. E. Moore and D. Yaron, J. Chem. Phys. **109**, 6147 (1998).

[55] Such large basis sets could be handled by direct CI methods, if the goal was to calculate a few low-lying states. However, the goal here is to calculate high-energy states that carry two-photon intensity and direct methods are not readily available.

[56] Inclusion of dielectric screening will also lower the free electron-hole pair states and increase the density of states.

Figures

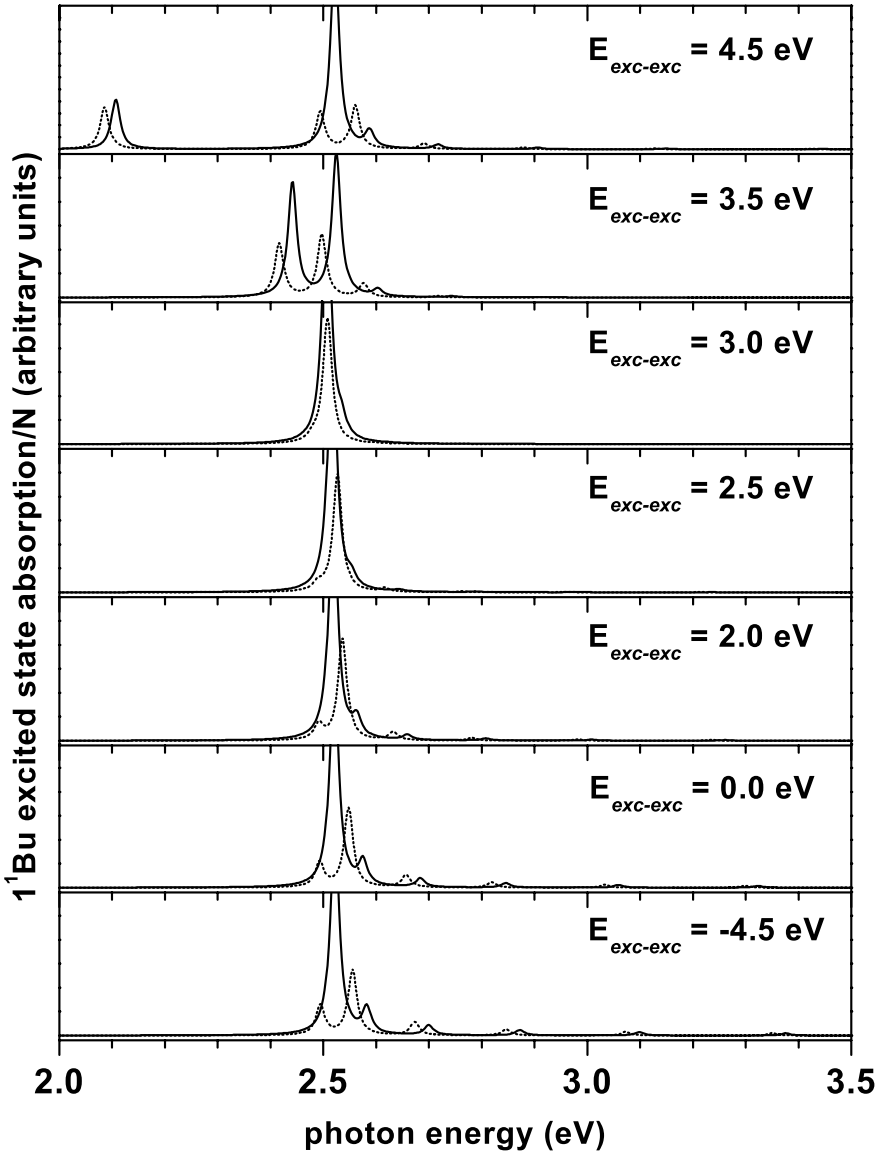

FIG. 1: Excited-state absorption from the 1^1B_u one-exciton state, for long chain Frenkel excitons with various $E_{\mathrm{exc-exc}}$, using periodic boundary conditions and N = 71 unit cells. The dotted line is K = 0, and the solid line is K = 2. The units of intensity are the same for all panels.

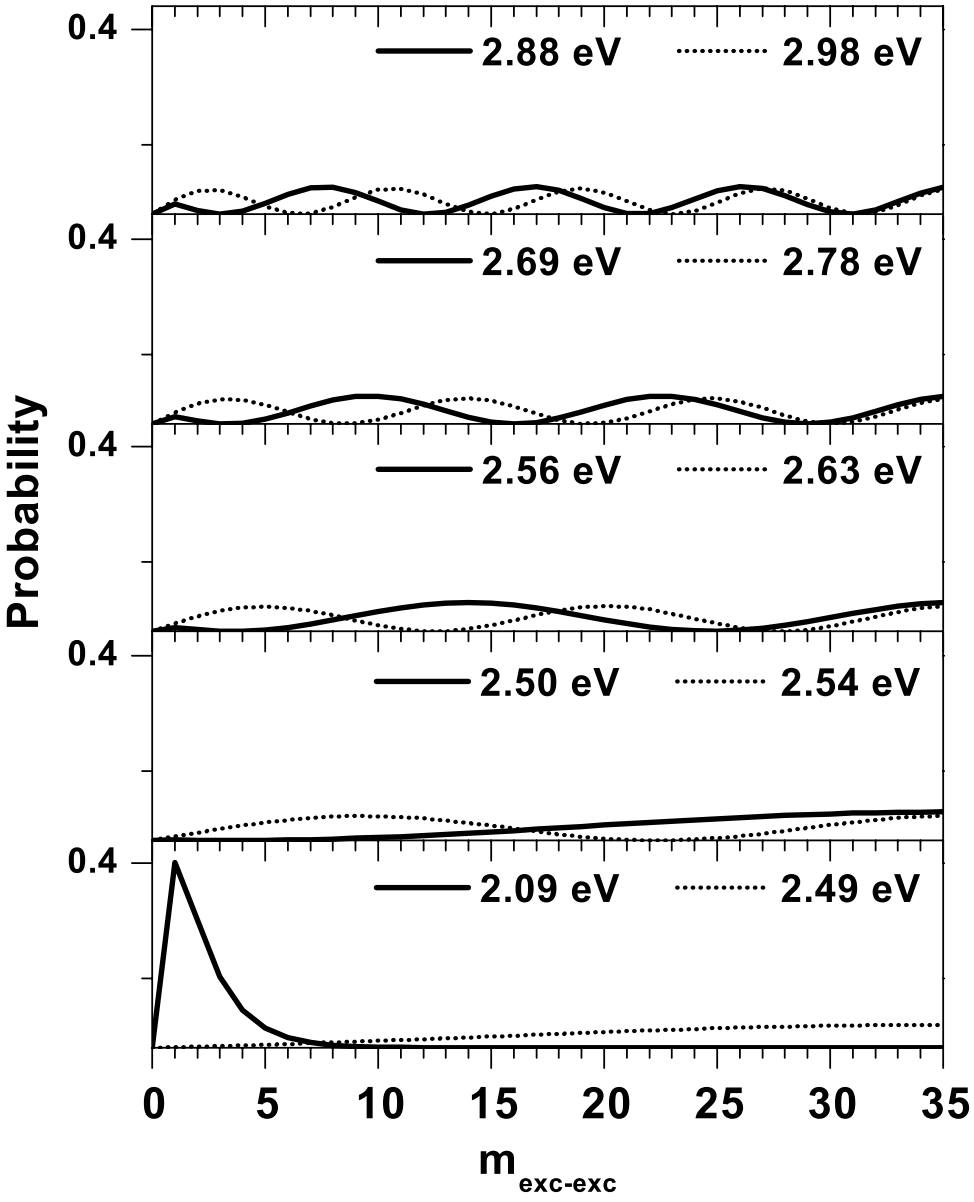

FIG. 2: Analysis of the wavefunctions for the states giving rise to the transitions in the spectra in Fig. 1 for $E_{\mathrm{exc-exc}} = 4.5$ (solid line) and 2.0 (dotted line). The K = 2 wavefunctions have the same form as K = 0. The probability density is shown as a function of exciton-exciton separation, $m_{\mathrm{exc-exc}}$.

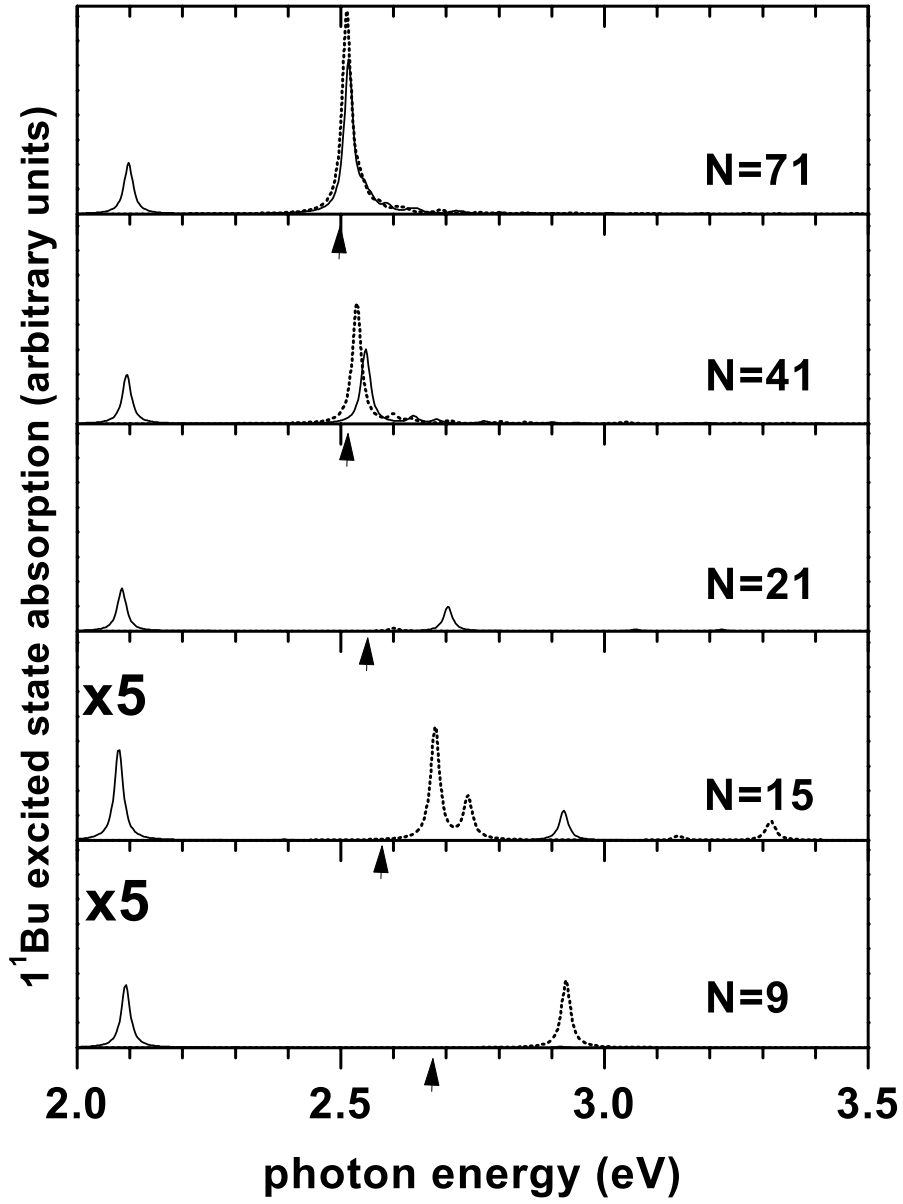

FIG. 3: Excited-state absorption from the 1^1B_u state, for Frenkel excitons with $E_{\mathrm{exc-exc}} = 4.5$ (solid line) or 2.0 (dotted line). The system is a linear chain with N unit cells. The 1^1B_u state energies are indicated by arrows. To allow comparison with chain length, the scale of the axes is the same for all panels, such that a constant height indicates the intensity is independent of chain length.

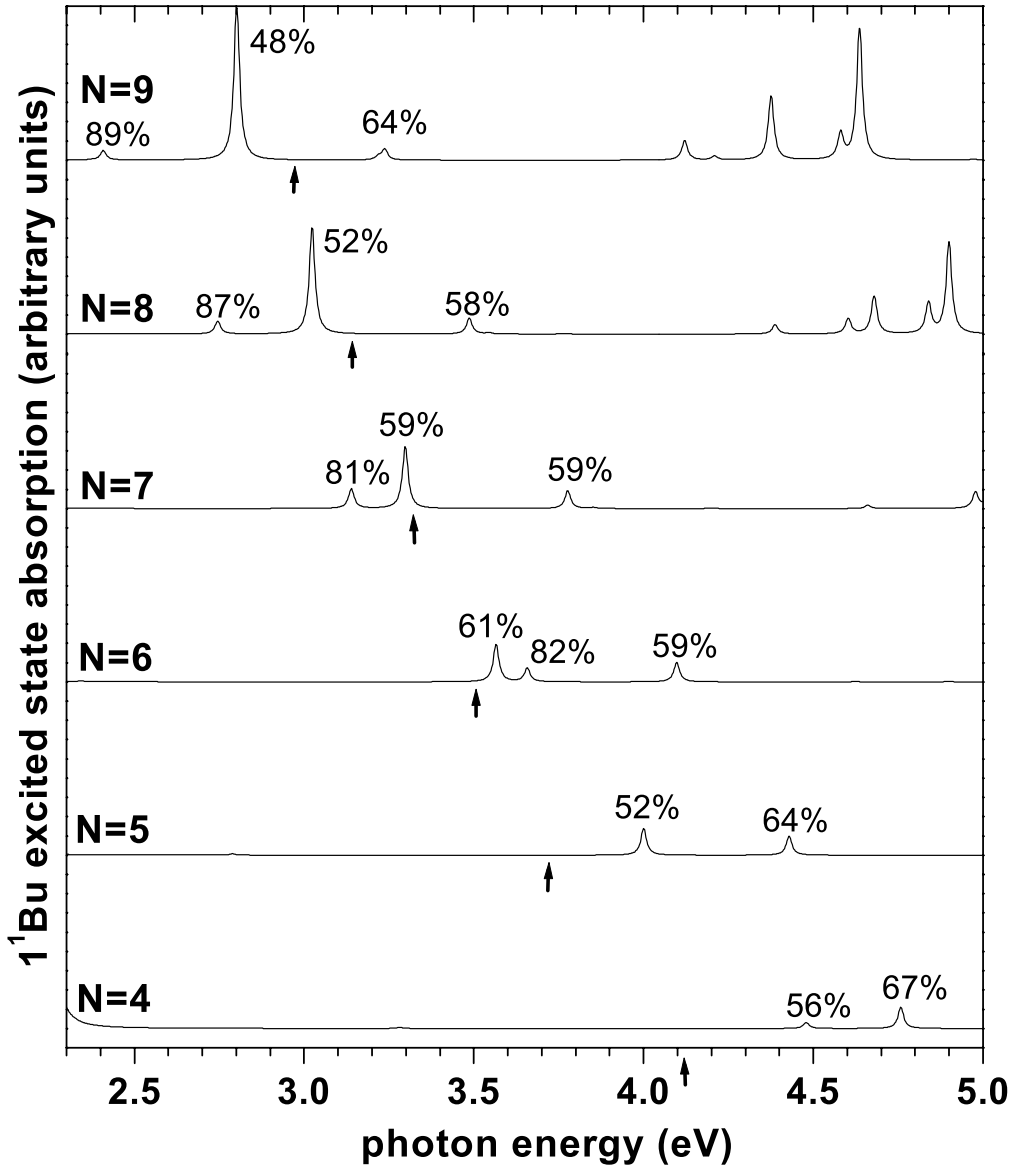

FIG. 4: Excited-state absorption for polyenes with N unit cells. The 1^1B_u state energies are indicated by arrows. The numbers above the peaks indicate the relative contribution of double electron-hole pair configurations to the excited state responsible for the transition.

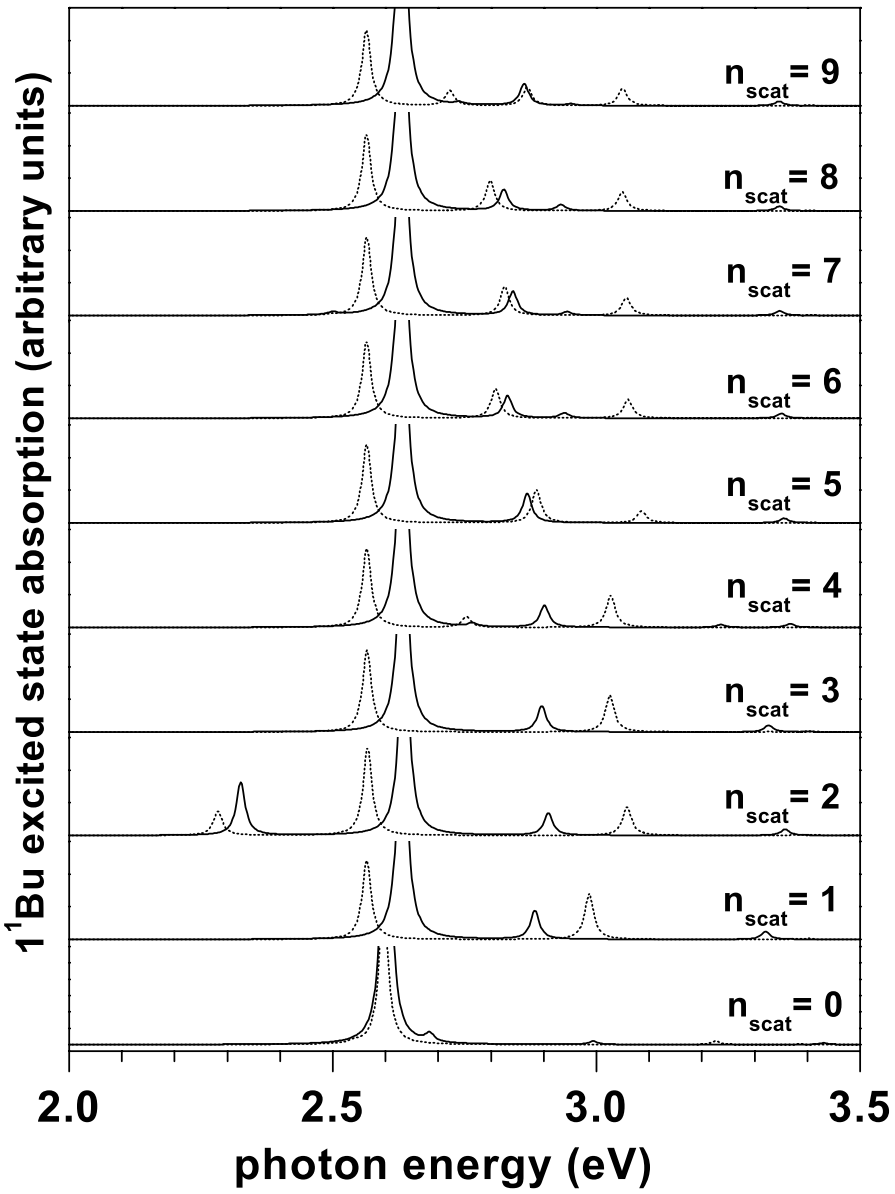

FIG. 5: Excited state absorption from the 1^1B_u state obtained for periodic polyacetylene chains with 71 unit cells and the indicated scattering regions, $n_{\rm scat}$. The dotted line is K = 0, and the solid line is K = 2.

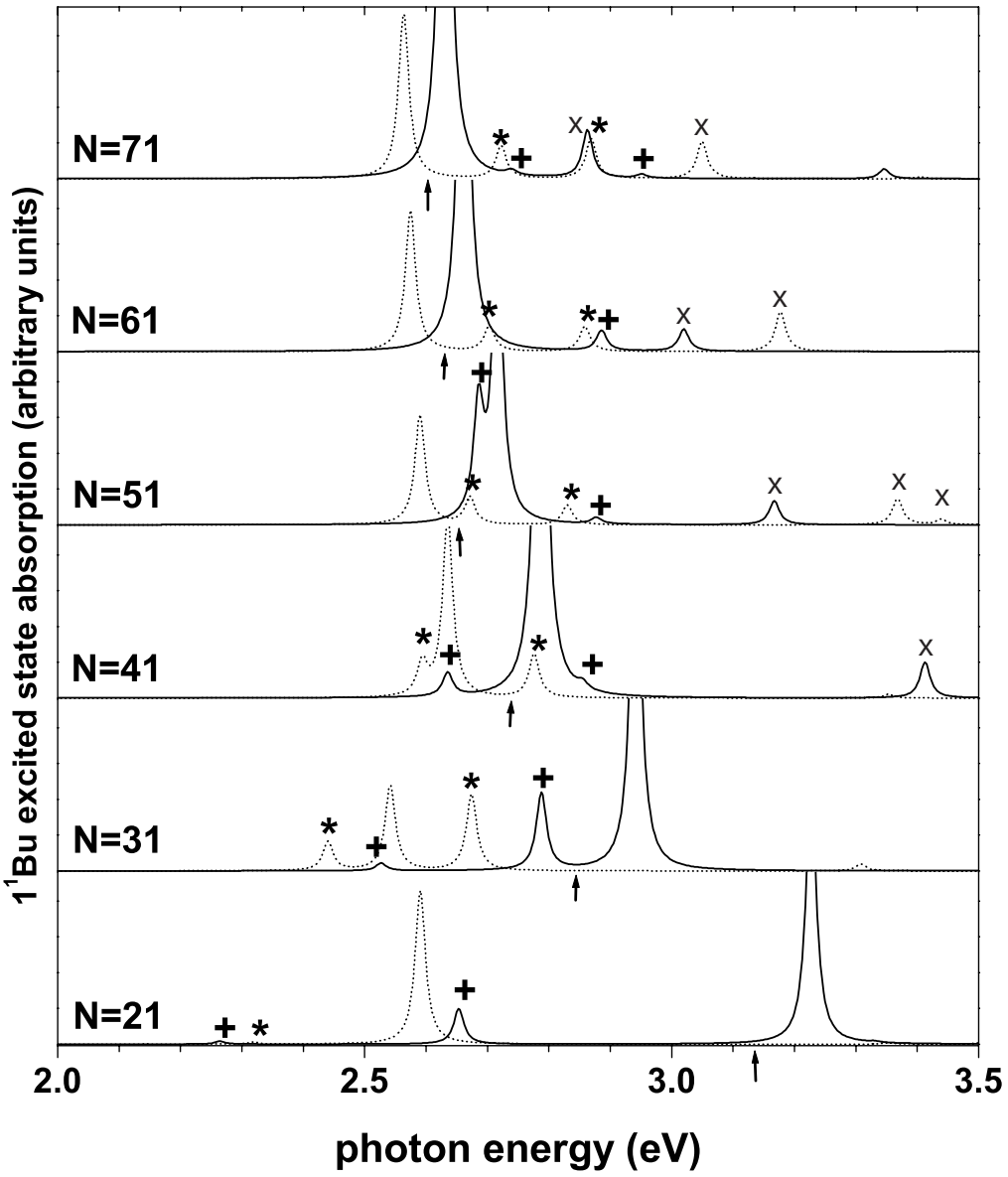

FIG. 6: Excited state absorption from the 1^1B_u state obtained for periodic polyacetylene chains with N unit cells and a scattering region of $n_{\rm scat} = 9$. The arrows indicate the 1^1B_u state energy, which is the expected long-chain position of the $2 \times \mathrm{E}_{1^1\mathrm{B_u}}$ peak. The dotted line is K = 0, and the solid line is K = 2. The peak labels are discussed in the text.

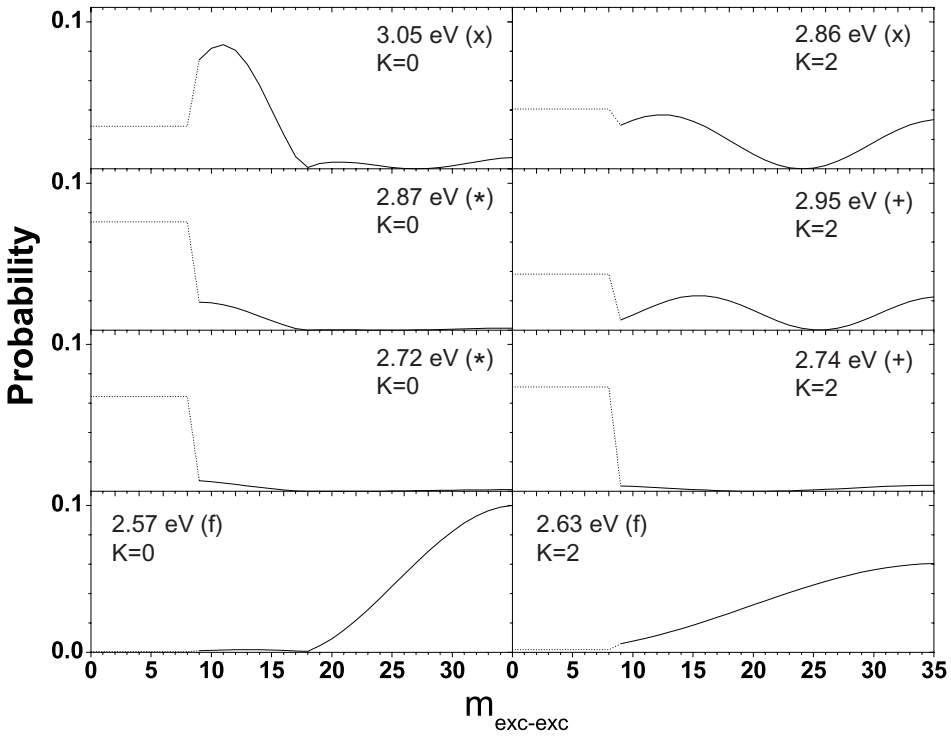

FIG. 7: Analysis of the wavefunctions for the states giving rise to the transitions in the $N = 71$ spectrum of Fig. 6. The probability density is shown as a function of exciton-exciton separation, $m_{\mathrm{exc-exc}}$. The dotted lines show the average probabilities within the scattering region. (Note that the probabilities due to single electron-hole configurations are not included.)

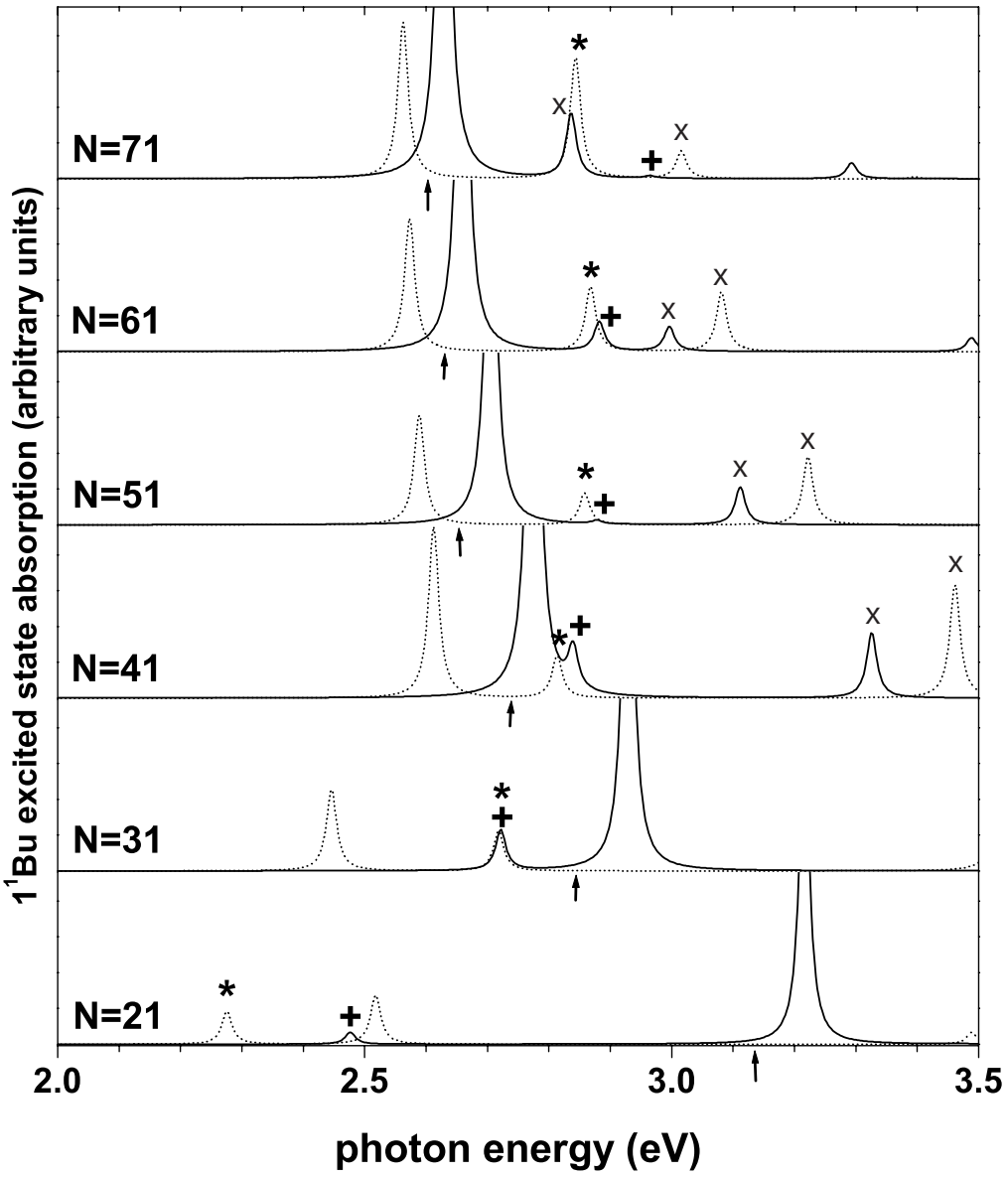

FIG. 8: Same as Fig. 6, but without inclusion of single electron-hole pair configurations in the calculation of the two-photon excited states (D-EOM).

Tables

TABLE I: Analysis of the wavefunctions giving rise to the transitions in the spectra of Fig. 6. The relative probabilities are listed for single electron-hole pair configurations (% singles) and for double electron-hole pair configurations within ($<n_{\rm scat}$) and outside ($>n_{\rm scat}$) of the scattering region.

	K = 0				**K = 2**			
N	**E(eV)**	**%sing**	**%doub**$<n_{\rm scat}$	**%doub**$>n_{\rm scat}$	**E(eV)**	**%sing**	**%doub**$<n_{\rm scat}$	**%doub**$>n_{\rm scat}$
71	2.57(f)	0.3	0.4	99.3	2.63(f)	0.6	1.6	97.8
	2.72(*)	37.8	58.2	4.0	2.74(+)	40.0	64.0	5.0
	2.87(*)	22.3	66.4	11.3	2.95(+)	30.9	34.4	34.6
	3.05(x)	16.2	26.0	57.8	2.86(x)	9.5	36.7	53.8
61	2.58(f)	0.6	0.8	98.6	2.66(f)	1.8	3.7	94.5
	2.70(*)	37.1	60.6	2.3	2.88(+)	31.7	54.7	13.6
	2.86(*)	29.8	66.7	3.5				
	3.18(x)	11.1	34.7	54.2	3.02(x)	11.6	16.5	71.9
51	2.59(f)	2.1	2.5	95.4	2.68(+)	24.0	60.5	15.5
	2.67(*)	34.9	61.2	3.9	2.72(f)	3.0	16.5	80.5
	2.83(*)	33.9	64.7	1.4	2.80(+)	41.5	54.1	4.4
	3.37(x)	34.0	38.8	27.2	3.16(x)	5.5	21.5	73.0
	3.44(x)	72.7	16.2	11.1				
41	2.59(*)	26.0	37.4	36.6	2.63(+)	22.8	76.7	0.5
	2.64(f)	10.2	29.9	59.9	2.79(f)	4.5	13.8	81.7
	2.77(*)	36.8	60.7	2.5	2.86(+)	42.8	44.4	12.8
					3.41(x)	9.1	36.1	54.8
31	2.44(*)	28.9	33.9	37.2	2.53(+)	17.9	82.1	0.0
	2.54(f)	9.3	54.9	35.8	2.79(+)	50.2	48.4	1.4
	2.67(*)	38.6	47.7	13.7	2.95(f)	2.1	14.6	83.3
	3.31	66.7	33.3	0.0				
21	2.32(*)	14.3	83.2	2.5	2.27(+)	13.2	86.8	0.0
					2.65(+)	54.9	45.1	0.0
	2.59(f)	16.4	47.7	35.9	3.23(f)	1.2	54.9	43.9